Assembly, Growth, and Catalytic Activity of Gold Nanoparticles in Hollow Carbon Nanofibers

Alessandro La Torre,[a] Maria del Carmen Giménez-López,[a] Michael W. Fay,[b] Graham A. Rance,[a] William A. Solomonsz, [a] Thomas W. Chamberlain,[a] Paul D. Brown[c] and Andrei N. Khlobystov*[a]

[a] *School of Chemistry, University of Nottingham, University Park, Nottingham, NG7 2RD, U.K.*

[b] *Nottingham Nanoscience and Nanotechnology Centre, University of Nottingham, University Park, Nottingham, NG7 2RD, U.K.*

[c] *Division of Materials, Mechanics and Structures, Department of Mechanical, Materials and Manufacturing Engineering, Faculty of Engineering, University of Nottingham, University Park, Nottingham, NG7 2RD, UK.*

Keywords: carbon nanofibres, gold nanoparticles, encapsulation, nanoparticle growth, nanoparticle assembly.

Abstract:

Graphitized carbon nanofibers (GNFs) act as efficient templates for the growth of gold nanoparticles (AuNPs) adsorbed on the interior (and exterior) of the tubular nanostructures. Encapsulated AuNPs are stabilized by interactions with the step-edges of the individual graphitic nanocones, of which GNFs are composed, and their size is limited to approximately 6 nm, while AuNPs adsorbed on the atomically flat graphitic surfaces of the GNF exterior continue their growth to 13 nm and beyond under the same heat treatment conditions. The corrugated structure of the GNF interior imposes a significant barrier for the migration of AuNPs, so that their growth mechanism is restricted to Ostwald ripening. Conversely, nanoparticles adsorbed on smooth GNF exterior surfaces are more likely to migrate and coalesce into larger nanoparticles, as revealed by in situ transmission electron microscopy imaging. The presence of alkyl thiol surfactant within the GNF channels changes the dynamics of the AuNP transformations, as surfactant molecules adsorbed on the surface of the AuNPs

diminished the stabilization effect of the step-edges, thus allowing nanoparticles to grow until their diameters reach the internal diameter of the host nanofiber. Nanoparticles thermally evolved within the GNF channel exhibit alignment, perpendicular to the GNF axis due to interactions with the step-edges and parallel to the axis because of graphitic facets of the nanocones. Despite their small size, AuNPs in GNF possess high stability and remain unchanged at temperatures up to 300 °C in ambient atmosphere. Nanoparticles immobilized at the step-edges within GNF are shown to act as effective catalysts promoting the transformation of dimethylphenylsilane to bis(dimethylphenyl)disiloxane with a greater than 10-fold enhancement of selectivity as compared to free-standing or surface-adsorbed nanoparticles.

Over the past decade, hollow carbon nanostructures filled with metal nanoparticles (NPs) have attracted a great deal of attention for their potential applications in different areas of nanotecnology [1-19] and biomedical sciences [24]. Different approaches have been proposed for inserting metal NPs into carbon nanostructures which act as passive containers[25-29], however, the control of the size and the position of encapsulated NPs, which are critical for catalysis or electronic applications, has not been realised. Up to date, only two examples of the encapsulation of preformed, free-standing metal NPs have been reported[25-27] showing that the size of the inserted NP can be significantly affected by the conditions of their encapsulation into the host-structure. Since metal nanoparticles, such as gold nanoparticles (AuNPs), exhibiting size-dependent physical and chemical properties are thermodynamically metastable; their applications are restricted to room temperature to avoid any undesirable NP transformations. There is a clear need for the development of new strategies broadening the temperature range of these applications, while controlling and retaining the NPs size. Our study aims at understanding the thermally driven growth process of metal NPs adsorbed outside and inside hollow graphitised carbon nanofibres (GNFs) revealing different mechanisms of thermal evolution of NPs. We demonstrate that the growth process and the nanoscale organisation of AuNPs depend on and can be controlled by the nature and strength of interactions between the guest-NPs and the host-nanocontainers.

Discussion

The growth of NPs adsorbed onto multiwall carbon nanotubes and other surfaces [30-32] or embedded in polymers[33] has been extensively investigated. Two possible mechanisms have been identified to be responsible for the growth: (A) Ostwald ripening and (B) particle migration followed by coalescence[34] (Figure 1). Transmission electron microscopy (TEM) is the only technique that is able to visualise directly metal NPs embedded in carbon or organic matrices and to observe their transformations in real time at the near-atomic level. However, so far the use of TEM is mainly restricted to *ex situ* measurements[35], which limit the level of information about the growth mechanism.[36] *In situ* TEM monitoring of physicochemical processes, however, must be applied with caution, as the energy of incident electrons of the electron beam (e-beam) may affect the kinetics or direction of a process under observation. Therefore, a real time monitoring of NP growth process in carbon nanostructures at nanoscale, which is critical for understanding the fundamental mechanisms of this process, still remains a challenge.

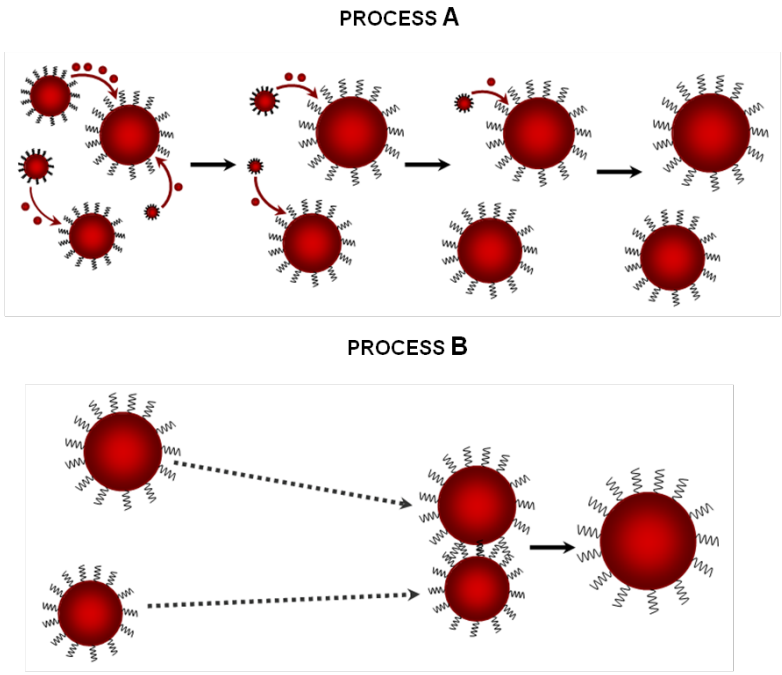

Figure 1. Schematic representation of the two different processes responsible for the growth of NPs: (A) Ostwald ripening of particles, where atoms or small clusters of atoms diffuse from smaller to larger NPs; and (B) the nanoparticle migration followed by coalescence. In both cases, the overall number of nanoparticles decreases as their average diameter increases.

Small dodecanethiol-stabilised gold NPs[37] (AuNPs) with a core diameter of 2.3±0.4 nm were selected for studying the growth process on GNF. Open, dry GNFs were added to a suspension of these AuNPs in a mixture of pentane/CO_2 in supercritical conditions (pressure 4000 bar, temperature 40 ^oC) to obtain the AuNP-GNF composite. Possessing very low viscosity and no surface tension, $scCO_2$ is able to penetrate the entire volume of GNFs and to deliver AuNPs into their channels as well as to deposit AuNPs on GNFs surface[38]. In the resultant composite material, the nanoparticles are randomly distributed on both surfaces (interior and exterior) of the hollow nanofibre (Fig. 3a). Detailed TEM imaging indicates that the size and shape distribution of adsorbed AuNPs remain virtually unchanged as compared to initial free-standing nanoparticles.

Unlike carbon nanotubes consisting of simple concentric tubes of graphene, the structures of the inner and outer GNF's surfaces are fundamentally different to each other. High-resolution TEM (HRTEM) imaging of the internal structure of GNFs produced by chemical vapour deposition (CVD) reveals a structure that can be described as a set of stacked cones of graphene (Figure 2a,c). HRTEM images of GNFs sidewalls clearly show planes of graphene oriented at an angle of *c.a.* 30º relative to the main GNF cylinder axis, and faint lines perpendicular to the GNF axis representing edges of cones that are spaced by 8-15 nm from each other, and thus creating a series of steps which can serve as “anchoring points” for molecules and nanoparticles inside GNF. In contrast, the outer surface of GNF consists of continuous atomically flat cylindrical layers of graphene (Figure 2a).

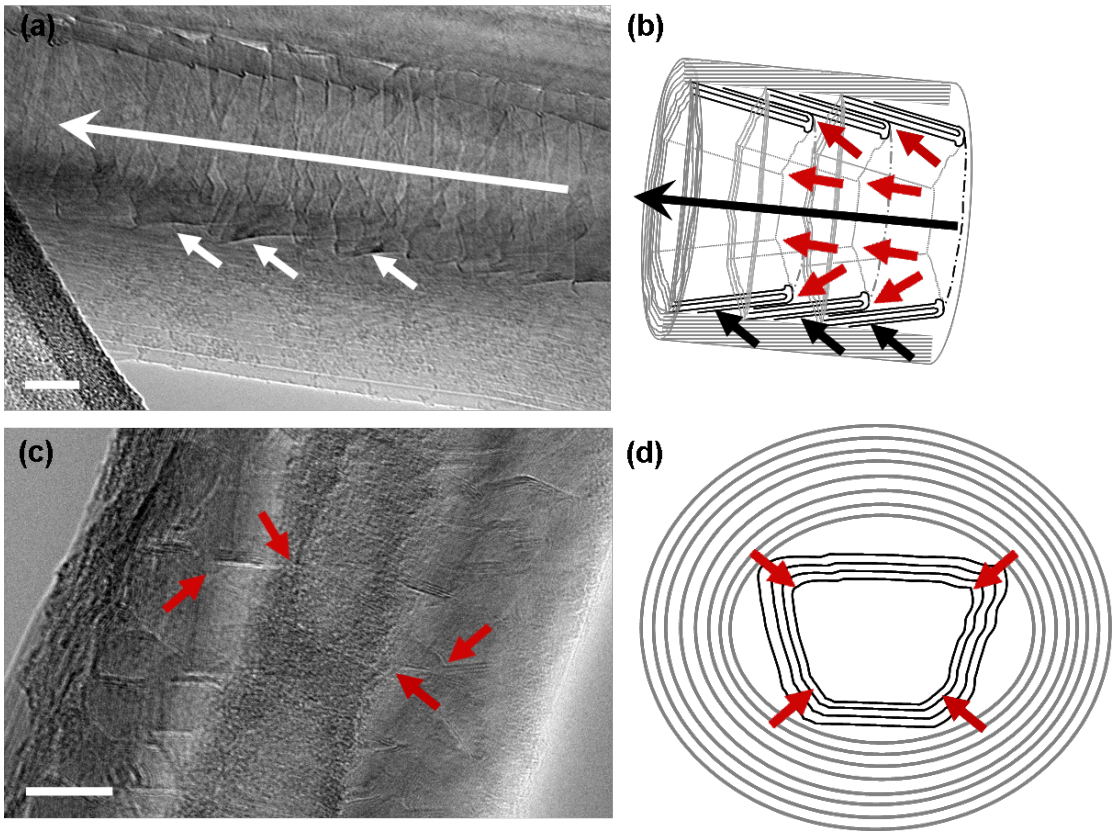

Figure 2. (a) Bright field transmission electron micrographs of the GNF showing the internal graphitic cone structure (short white arrows) which is formed by a few layers of graphene. In contrast, the external surface consisting of continuous cylindrical layers of graphene is atomically smooth. (b) Schematic representation of a GNF. The cone wall structure is indicated by short black arrows, the long arrow indicates the main axis of the GNF and the red arrows show the possible anchoring points on the nanocone step-edges. (c) Bright field transmission electron micrograph of GNF showing the facets of the cone step-edges. The red arrows indicate the four vertex of a set of stacked cones. (d) Schematic representation of a section of GNF. The red arrows indicate the vertex of the facets of the cone step-edges. Scale bars are 20 nm in (a) and 50 nm in (c). TEM image acquisition was performed using an accelerating voltage of 100 kV.

Thermal energy activates growth of nanoparticles in AuNP-GNF composite. AuNP-GNF samples heated in vacuum (inside TEM column using a heated-stage TEM holder or in a sealed evacuated tube in a furnace) at 300 ºC for 2 hours exhibit a binary mixture of nanoparticles (Figure 3d-f). Initial monodispersed 2.3 nm AuNPs (Figure 3a) transform into two distinct groups: 6.4±0.4 nm AuNPs and 13.4±0.6 nm AuNPs. Furthermore, the set of larger nanoparticles appears to be positioned on GNFs surface, while smaller ones are inside GNF. Considering that TEM images are

projections of 3D nanostructures, however, the assignment of AuNP location is not entirely unambiguous at this stage.

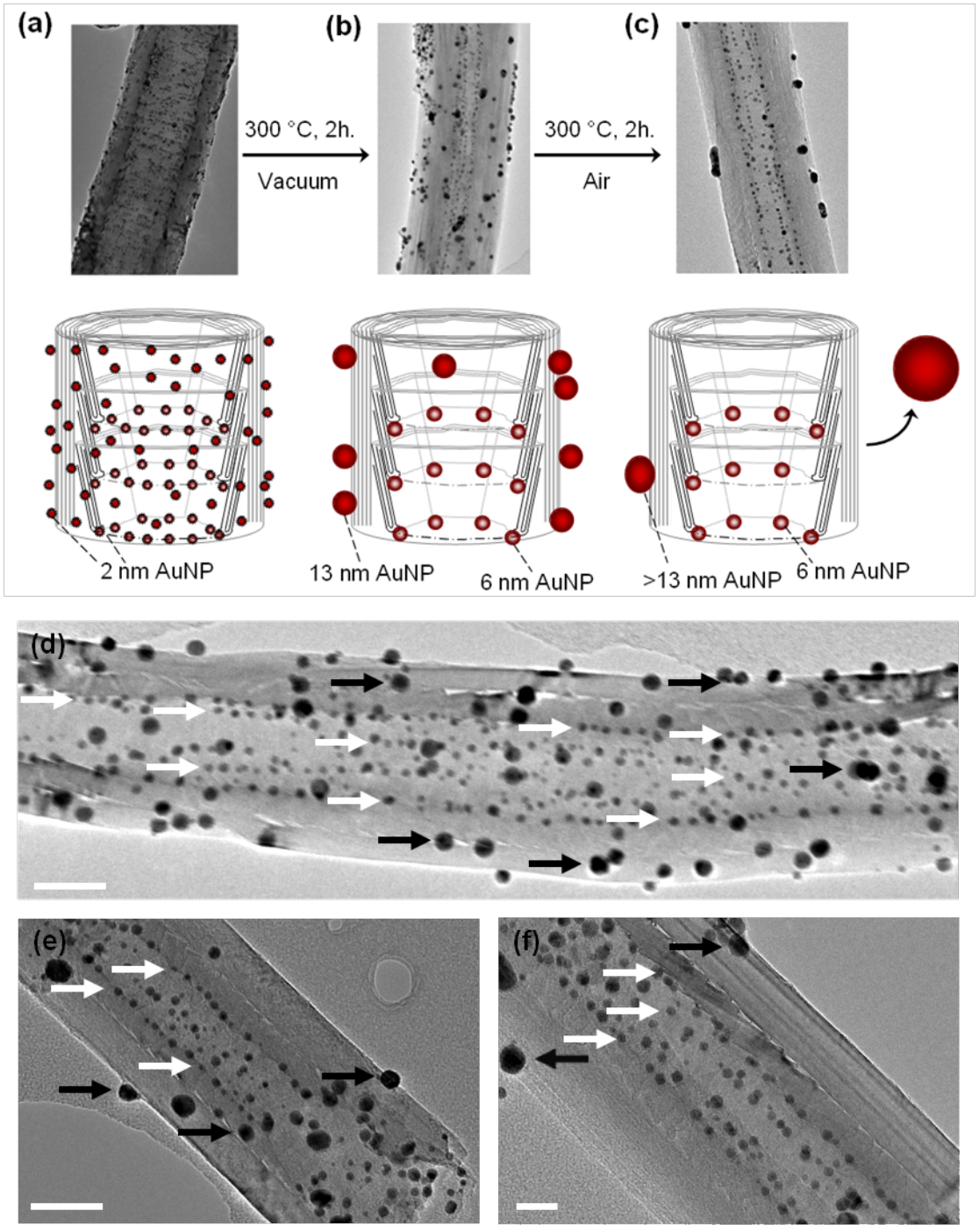

Figure 3. Bright field TEM images (above) and schematic diagrams (below) illustrating the AuNPs adsorbed on the GNF outer surface (dark red) and anchored at the graphitic step-edges within GNF (light red) (a) immediately after the deposition of 2.3 nm AuNPs, (b) after heating the AuNP-GNF composite in vacuum at 300 ºC for 2 hours, and (c) after additional heating at 300 ºC in air for further two 2 hours post heating in vacuum. Nanoparticles formed inside are stable and retain their size (6 nm) even at elevated temperatures, while external nanoparticles are prone to migration and

desorption from GNF (c). Bright field TEM image of AuNPs grown from 2.3 nm AuNP at 300 ºC on a heated-stage TEM holder (d) and in a furnace (e, f) in vacuum. White and black arrows indicate AuNPs formed within the GNF cavity and on the GNF exterior surface, respectively. Scale bars are 50 nm in (d,e) and 20 nm in (f). The voltage used for this image was A 100 KeV.

High-angle annular dark-field (HAADF) scanning transmission electron microscopy (STEM) imaging of a AuNP–GNF composite sample, heat treated at 300 °C in vacuum, at different tilt angles clearly shows that only the 6 nm AuNPs are located in the internal cavity of the GNF (to a level of 500 NPs 3 μm□1), forming linear arrangements along the nanofiber axis. In contrast, AuNPs with diameters g13 nm are randomly distrib- uted on the outer surface of the GNF (Figure 4).

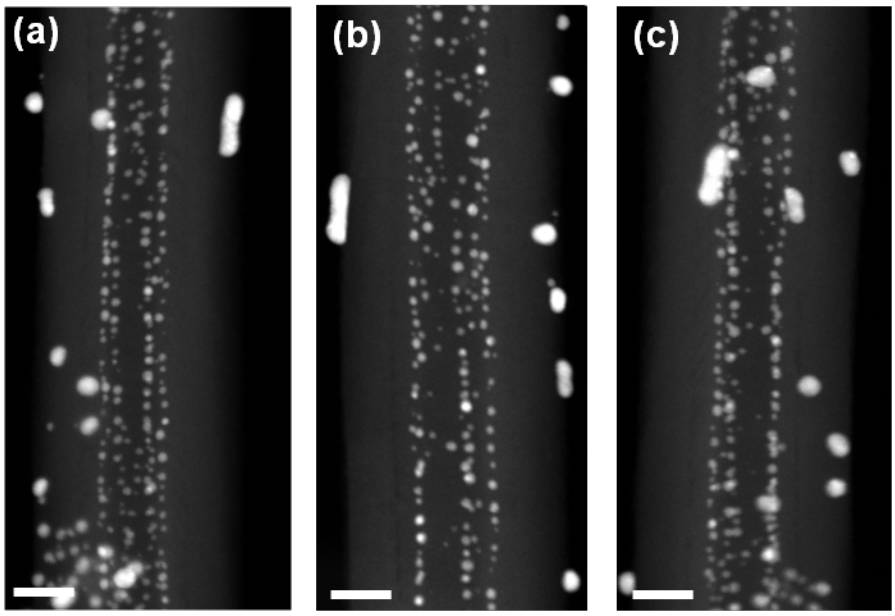

Figure 4. High angular angle dark field STEM images of thermally evolved AuNPs for different tilt angles of the host GNF +60º (a), 0º (b) and -60º (c). During the tilt series, 6 nm AuNPs remain located within the GNF cavity while 13 nm and larger AuNPs change their positions with respect to the GNF interior. The scale bars are 50 nm. The TEM image acquisition was performed using an accelerating voltage of 100 kV.

To ensure that the e-beam of TEM does not create any changes in the structure of the specimen, we utilised a low flux and low energy (100 keV) e-beam, and a minimum exposure time to the e-beam (only during the image capture). Under our imaging conditions no observable changes are induced by the e-beam in the specimen, which ensures that the images represent the true structure of the specimen. However, when

AuNP-GNF composites are exposed to a high flux (*c.a.* 50 pA/cm^2) of the high energy e-beam (200 keV) for extended periods of time, the growth of nanoparticles can be triggered by the e-beam even at room temperature (Supporting Information, Figure S4). Interestingly, AuNPs inside GNF exposed to the intensive e-beam radiation grow to the same maximum size of *c.a.* 6 nm as in the thermally activated experiments. These observations that regardless the source of energy providing the driving force of AuNPs transformation (heat or e-beam), AuNPs inside GNF always grow to the same maximum size in vacuum, clearly indicate that the growth is controlled by the local structure of graphene layers of the nanofibre.

In situ TEM imaging of the thermally activated transformation of AuNPs on the corrugated interior and the smooth exterior of GNFs in real time provides important information about the NP growth mecha- nisms. Our observations show that the processes of Ostwald ripening and nanoparticle coalescence coexist
in AuNP□GNF structures. Ripening (mechanism A, Figure 5) is observed typically for smaller AuNPs (e6 nm), where clusters of gold atoms diffuse from smaller AuNPs to larger AuNPs (Supporting Information). The migration and coalescence mechanism (B, Figure 5) appears to be dominant for AuNPs with sizes larger than 6 nm (Supporting Information). Since AuNPs adsorbed on the atomically smooth GNF exterior can migrate freely, they continue their growth beyond 6 nm. In contrast, migration of nanoparticles within GNF is inhibited due to the corrugated nature of the inner surface.
It is considered that the corrugated interior of the GNFs restricts the migration of nanoparticles within the cavity and thus precludes their growth via coalescence, so that Ostwald ripening remains the only possible growth mechanism for AuNPs inside the nanofiber. For the GNFs in this study, the typical height of the step- edges formed by the rolled-up graphene sheets is 3.3 (0.2 nm, and hence the surface area of contact between the AuNPs and GNF is maximized when the AuNPs are located at the apexes of the graphitic facets of step-edges (Figures 3b and 4a,d), which leads to a drastic enhancement in the van der Waals interactions between the AuNPs and the carbon nanostructure.33 This favorable interaction, occurring at the step-edges, immobilizes the nanoparticles, thus precluding their migration and thus growth above 6 nm in diameter.

The stability of the AuNPs thermally evolved on or in the GNFs in vacuum was examined in ambient environment by heating samples at 300 °C in atmospheric air (Figure 2c). Surface-adsorbed nanoparticles contin- ued their growth beyond 13 nm when the AuNP–GNF composite was heated in air, often becoming elongated and detached from the GNF (Supporting Information, Figure S3), while AuNPs adsorbed inside the GNF retained their size and shape.

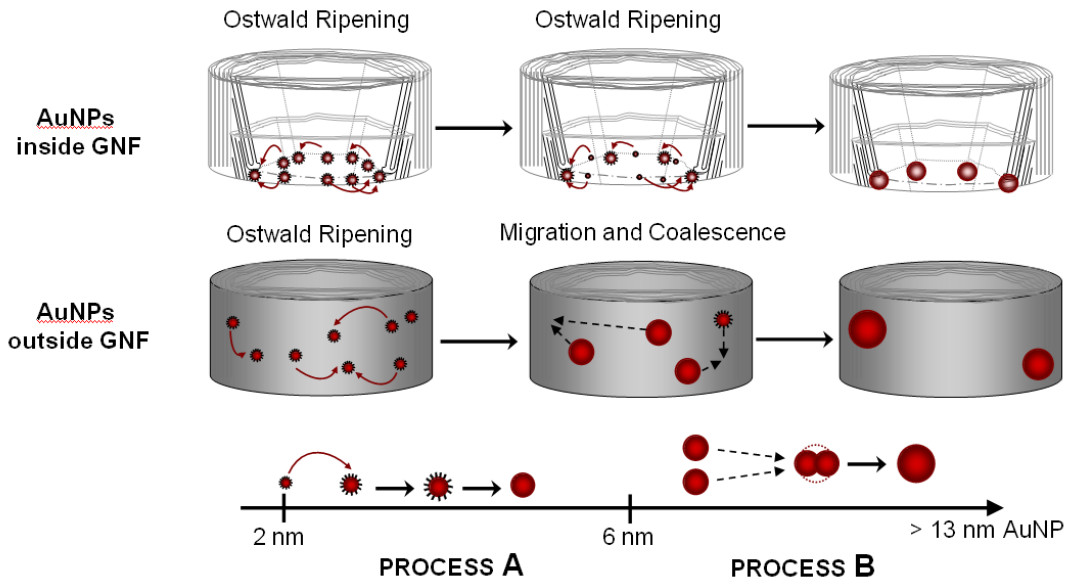

Figure 5. Schematic representations of the observed growth mechanisms of AuNPs in the GNFs internal cavities (above) and on the GNFs exteriors (below). Ostwald ripening and nanoparticle migration events are indicated by solid and dashed arrows respectively.

X-ray photoelectron spectroscopy (XPS) indicates complete removal of alkylthiol stabilizer from the AuNP GNF composite in vacuum, so that direct contact between the metal surface of the nanoparticles and the GNF is established. This contact appears to be particularly effective at stabilizing the AuNPs adsorbed at step-edges. Nor- mally, small metal nanoparticles (a few nanometers in diameter) are unstable at elevated temperature, but the 6 nm AuNPs adsorbed within the nanofiber exhibit remarkable stability up to 300 °C (Figures 2c, 4, and 6d).

Alkylthiol molecules, which have a high affinity for the surface of gold and hence are commonly employed as a protecting capping layer for AuNPs synthesized in solution, can influence the interactions between AuNPs and GNFs. When free-standing, alkylthiol-stabilized 2.3 nm AuNPs are inserted into GNFs from an scCO2 solution, the stabilizer is also inserted into the nanofiber, as confirmed by XPS and thermal gravi- metric analysis (TGA) measurements (Supporting In- formation, Figures S6-S10). During heating in vacuum, the surfactant molecules are fully and rapidly removed from the AuNP□GNF composite, but when AuNP–GNF is heated under atmospheric pressure, some of the alkylthiol remains inside the GNF. It is likely that the stabilizer impedes intimate contact between the metal surface of the AuNP and GNF that is required for stabilizing the nanoparticles at the step-edges. This leads to the continuous, unrestricted growth of the nanoparticles via migration and coalescence, until they reach the size of the internal cavity of the host GNF (Figure 6a,b).

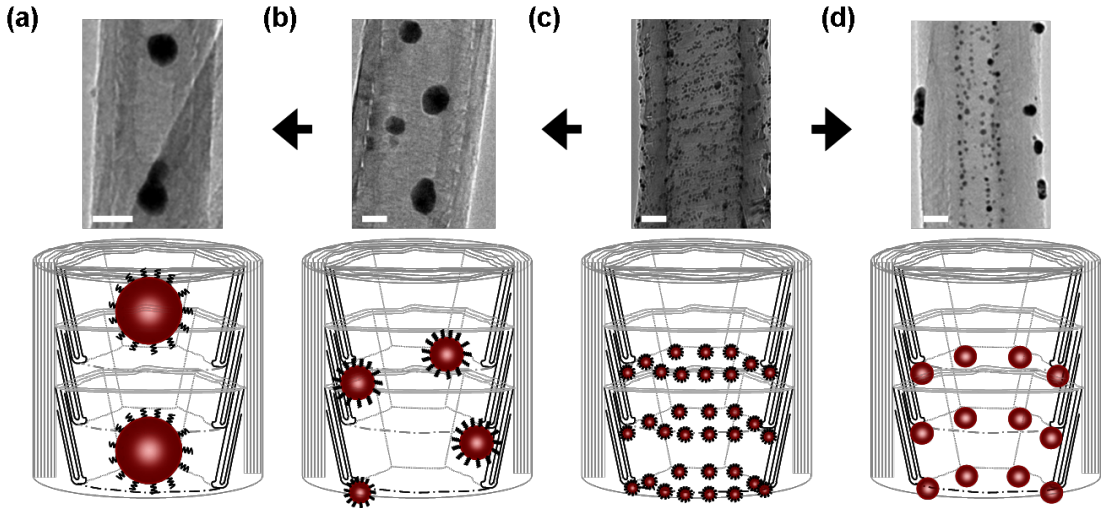

Figure 6. Bright field images (above) and schematic diagrams (below) of AuNP in GNFs heated in air at 300 °C (a) and 200 °C (b) both for 2 hours, AuNP-GNF immediately after insertion 2.3 nm AuNPs from $scCO_2$ (c) and AuNP evolved in GNF by heated in vacuum at 300 °C for 2 hours. Scale bar in (a) 50 nm and 20 nm in (b-d). The TEM imaging acquisition was performed using an accelerating voltage of 100 kV

Furthermore, in addition to structural factors, elec- tronic factors may also play an important role in the stabilization of AuNPs. A recent study has demon- strated that the electrostatic interactions arising from charge transfer between the graphitic surface and gold nanoparticle can influence the size of the growing AuNPs.34 It is interesting

that the average size of nanoparticles was found to correlate with the number of graphene layers, with larger nanoparticles forming on thicker stacks of graphene.34 Since in GNFs the tubular outer layer consists of a much thicker stack of graphene than the internal cones (Figure 3), our ob- servation that smaller AuNPs are formed inside the nanofiber is consistent with the model developed for flat graphitic surfaces.34

In contrast to the random distribution of AuNPs on the GNF exterior surface, the nanoparticles inside the GNF form well-defined rows and columns. The rows are oriented perpendicular to the GNF cylinder axis and spaced by 6□9 nm from each other, which is commen- surate with the lengths of the steps formed by the stacked cones. The columns of AuNPs, parallel to the GNF axis, reflect the faceted nature of the interior nanocone surface, as nanoparticles are preferentially positioned at the apexes of the facets (Figure 4a,d). In addition to the fact that the internal surface of the GNF has a significant stabilizing effect on the metal nano- particles, which remain unchanged in air at 300 °C for over 2 h, the internal corrugations of the nanofiber serve as effective templates for ordering AuNPs in two directions, parallel and perpendicular to the GNF axis. Although the thermal treatment allows desorption from the GNF of the vast majority of the external AuNPs (Supporting Information, Figure S3), a small number of

NPs still remain adhered to the nanofibers' outer sur- face. For specific practical applications of the NP□GNF composite, however, it is critical to ensure that all of the NPs are located inside. Hence, a selective procedure for the removal of the surface NPs, without affecting the encapsulated NPs, is highly desirable. We discovered that large nanoparticles could be effectively removed from the GNF surface by ultrasound. Thermally evolved AuNP□GNF composites subjected to an ultrasonic treatment in ethanol show selective desorption of AuNPs from the exterior surface (Supporting Informa- tion, Figure S11). Powder X-ray diffraction performed on bulk samples of ultrasound-cleaned AuNP□GNF indicates that only nanoparticles with a diameter of 6.2 nm (corresponding to the internal AuNPs) remain adsorbed (Supporting Information, Figure S11), which is consistent with TEM imaging (Figure 6d).

Nanoparticles inserted into GNF from supercritical fluid were shown to act as catalytic centers for the oxidation of silane by hydrogen peroxide (Scheme 1). The reaction of dimethylphenylsilane (1) leads to two products: dimethylphenylsilanol (2) and bis(dimethyl- phenyl)disiloxane (3). While the selectivity of gold nanoparticles

adsorbed on the GNF outer surface is similar to that of free-standing AuNPs, favoring the formation of product 2, the distribution of reaction products changes drastically for AuNPs encapsulated inside the nanofiber (Scheme 1). The enhanced pro- duction of 3 inside GNF can be explained by an increased local concentration of reactants within the GNF cavity, which is a general phenomenon observed in nanoreactors.[2] The formation of product 3 requires the collision of two dimethylphenylsilanol molecules, and therefore, any increase of concentration caused by the confinement in GNF will favor the formation of bis(dimethylphenyl)disiloxane. This control of chemical processes observed in GNFs illustrates the potential of carbon nanofibers as reaction nanovessels which are currently explored for preparative reactions by ourselves and others.[1,23]

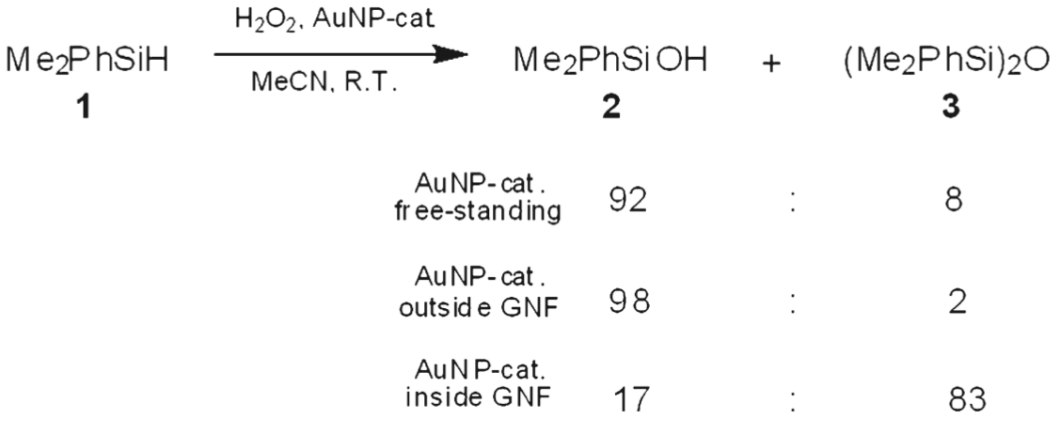

Scheme 1. AuNP-catalyzed silane oxidation by H_2O_2 and the effects of nanoparticle encapsulation in GNF on the distribution of products.

Conclusion

Graphitized carbon nanofibers possessing different internal and external graphitic surfaces have been demonstrated as efficient host structures for nanopar- ticles of gold. Transformation of the deposited NPs can be activated directly on the GNFs using heat or an electron beam as the source of energy to promote the growth of the AuNPs. In situ TEM imaging allowed the two key mechanisms responsible for nanoparticle growth to be established: Ostwald ripening and migra- tion followed by coalescence. The first process is prevalent for nanoparticles with diameters of 6 nm or

less, whereas the second is significantly more impor- tant for larger NPs on the exterior surface. Graphitic step-edges forming the internal surface of GNF act to stabilize small NPs, restricting their migration and thus limiting their growth to 6 nm. Despite the fact that small metal nanoparticles are typically highly labile and metastable, AuNPs formed within GNFs exhibit no changes at temperatures as high as 300 °C. The pres- ence of surfactant molecules (alkylthiols) within the GNF, however, can impede the interaction between AuNPs and the GNF, reducing the stabilizing effect of the graphitic step-edges and promoting further growth of the nanoparticles inside the GNF, being limited only by the space available within the nanofiber.

The ability to control the size and stability of nano- particles by encapsulation in hollow nanofibers offers a new methodology for improving their thermal stability and for enhancing the functional performance of these otherwise metastable nanostructures. An additional benefit of the confinement within the GNF nanocon- tainers is the spontaneous ordering of NPs in two directions;across and along the GNF's channel. The ability to form rows and columns of well-organized equidistant and highly stable nanoparticles is highly desirable for catalytic, spintronic, data storage and photovoltaic applications.

Experimental Section

GNFs produced by chemical vapor deposition were pur- chased from Applied Science, USA. All other reagents and solvents were purchased from Sigma-Aldrich, UK, and used without further purification. Water was purified (>18.0 MΩ cm) using a Barnstead NANOpure II system. The experimental procedures followed for the preparation, insertion, and growth of the 2.3 nm AuNPs in vacuum, air, and in situ TEM are de- scribed in detail in the Supporting Information. The preparation of AuNPs required glassware to be cleaned with a mixture of concentrated hydrochloric and nitric acids (3:1 v/v, “aqua regia”), rinsed with deionized water, further cleaned with potassium hydroxide in methanol, and finally rinsed thoroughly with deionized water prior to use. HRTEM was performed using a JEOL 2100F transmission electron microscope (field emission electron gun source, information limit 0.19 nm) using an accelerating voltage of 100 or 200 kV. TEM specimens were prepared by casting several drops of methanolic suspensions of AuNP-GNF onto copper-grid or nickel-

grid mounted “holey” carbon films and drying under a stream of nitrogen. The annular-ring used for the in-situ TEM experiment was a Gatan 652 Double tilt heating holder. Acquisition of tilt series was performed using a Gatan 916 tomography holder and a Gatan double tilt beryllium holder. High angle annular dark field images were acquired using a JEOL Digital STEM System. Statistical analysis was performed for each sample using Gatan Digital Micrograph software. By tilting AuNP-GNF composites along the main nanofibre axis, in different regions of the specimen, the amount of encapsulated AuNPs was estimated for each area and averaged across the entire sample. Powder X-ray diffraction patterns were recorded using a Bruker D8 Advanced X-ray diffractometer equipped with Cu KR source (λ = 1.5418 Å). Thermogravimetric analysis was determined using a TA Instrument equipped with a SDT Q600 analyzer under flowing air at a rate of 10 °C/min up to 800 °C. X-ray photoelectron spectra were recorded using a Kratos AXIS ULTRA with monochromated Al KR radiation (10 kV anode potential, 15 A emission current) in fixed analyzer transmission mode (80 eV pass energy). Distribution of products in the reaction of AuNP-catalyzed oxidation of dimethylphenyl-silane was determined by GC-MS, VG Autospec in EI (Supporting Information, section S12).

Acknowledgements

The authors thank the European Science Foundation, the Royal Society, Marie Curie Fellowship and the University of Nottingham for supporting this research, the Nottingham Nanoscience and Nanotechnology Centre for access to TEM facilities and Dr Nigel Neate and Keith Dinsdale for technical support.
The authors acknowledge the use of the Kratos Axis ULTRA XPS in the School of Chemistry and Emily Smith for running the samples and helpful discussions on data interpretation.

References

1. Serp, P.; Castillejos, E. Catalysis in Carbon Nanotubes. ChemCatChem 2010, 2, 41–47.
2. Pan, X.; Bao, X. The Effects of Confinement Inside Carbon Nanotubes on Catalysis. Acc. Chem. Res. 2011, 44, 553–562.

3. Datta, S.; Marty, L.; Cleuziou, J. P.; Tilmaciu, C.; Soula, B.; Flahaut, E.; Wernsdorfer, W. Magneto-Coulomb Effect in Carbon Nanotubes Quantum Dots Filled with Magnetic Nanoparticles. Phys. Rev. Lett. 2011, 107, 186804.
4. Li, B. D.; Wang, C.; Yi, G. Q.; Lin, H. Q.; Yuan, Y. Z. Enhanced Performance of Ru Nanoparticles Confined in Carbon Nanotubes for CO Preferential Oxidation in a H_2-Rich Stream. Catal. Today 2011, 164, 74–79.
5. Cleuziou, J. P.; Wernsdorfer, W.; Ondarcuhu, T.; Monthioux, M. Electrical Detection of Individual Magnetic Nanoparti- cles Encapsulated in Carbon Nanotubes. ACS Nano 2011, 5, 2348–2355.
6. Kang, J. W.; Kim, K. S.; Kwon, O. K.; Hwang, H. J. Linear Nanomotor Based on Electromigration of a Nanoparticle Encapsulated in a Carbon Nanotube. Nanosci. Nanotech- nol. 2011, 11, 1573–1576.
7. Wang, J.; Beeli, P.; Ren, Y.; Zhao, G. M. Giant Magnetic Moment Enhancement of Nickel Nanoparticles Eembedded in Multiwalled Carbon Nanotubes. Phys. Rev. B 2010, 82, 193410.
8. Roa, D. B.; Barcelos, I. D.; de Siervo, A.; Pirota, K. R.; Lacerda, R. G.; Magalhaes-Paniago, R. Observation of Ferromagnet- ism in PdCo Alloy Nanoparticles Encapsulated in Carbon Nanotubes. Appl. Phys. Lett. 2010, 96, 253114.
9. Guo, S. J.; Pan, X. L.; Gao, H. L.; Yang, Z. Q.; Zhao, J. J.; Bao, X. H. Probing the Electronic Effect of Carbon Nanotubes in Catalysis: NH_3 Synthesis with Ru Nanoparticles. Chem.; Eur. J. 2010, 16, 5379–5384.
10. Gan, L.; Lv, R.; Du, H. D.; Li, B. H.; Kang, F. Y. Highly Dispersed Pt Nanoparticles by Pentagon Defects Introduced in Bam- boo-Shaped Carbon Nanotube Support and Their En- hanced Catalytic Activity on Methanol Oxidation. Carbon 2009, 47, 1833–1840.
11. Qin, Y.; Liu, L. F.; Yang, R. B.; Gosele, U.; Knez, M. General Assembly Method for Linear Metal Nanoparticle Chains Embedded in Nanotubes. Nano Lett. 2008, 8, 3221–3225.
12. Monch, I.; Leonhardt, A.; Meye, A.; Hampel, S.; Kozhuharova- Koseva, R.; Elefant, D.; Wirth, M. P.; Buchner, B. Synthesis and Characteristics of Fe-Filled Multi-Walled Nanotubes for Biomedical Application. Proc. Int. Conf. Nanosci. Tech. 2007, 61, 820–824.
13. Banhart, F.; Grobert, N.; Terrones, M.; Charlier, J. C.; Ajayan, P. M. Metal Atoms in Carbon Nanotubes and Related Nanoparticles. Int. J. Modern Phys. B 2001, 15, 4037–4069.
14. Ratanatawanate, C.; Xiong, C.; Balkus, K., Jr. Fabrication of PbS Quantum Dot Doped TiO_2 Nanotubes. ACS Nano 2008, 2, 1682–1688.
15. Ratanatawanate, C.; Tao, Y.; Balkus, K., Jr. Photocatalytic Activity of PbS Quantum Dot/TiO_2 Nanotube Composites. J. Phys. Chem. C 2009, 113, 10755–10760.
16. Tsang, S. C.; Chen, Y. K.; Harris, P. J. F.; Green, M. L. H. A Simple Chemical Method of Opening and Filling Carbon Nanotubes. Nature 1994, 372, 159–162.
17. Ajayan, P. M.; Iijima, S. Capillarity-Induced Filling of Carbon Nanotubes. Nature 1993, 361, 333–334.
18. Ajayan, P. M.; Colliex, C.; Lambert, J. M.; Bernier, P.; Barbedette, L.; Tence, M.; Stephan, O. Growth of Manganese Filled Carbon Nanofibres in the Vapour-Phase. Phys. Rev. Lett. 1994, 72, 1722–1725.
19. Ugarte, D.; Chatelain, A.; de Heer, W. A. Nanocapillarity and Chemistry in Carbon Nanotubes. Science 1996, 274, 1897– 1899.
20. Huang, H.; Kajiura, H.; Murakami, Y.; Ata, M. Metal Sulphide Catalyzed Growth of Carbon Nanofibres and Nanotubes. Carbon 2003, 41, 615–618.
21. Costa, P. M. F. J.; Sloan, J.; Rutherford, T.; Green, M. L. H. Encapsulation of Re_XO_y Clusters within Single-Walled Car- bon Nanotubes and Their in Tubulo Reduction and Sinter- ing to Re Metal. Chem. Mater. 2005, 17, 6579–6582.

22. Wang, C.; Guo, S.; Pan, X.; Chen, W.; Bao, X. Tailored Cutting of Carbon Nanotubes and Controlled Dispersion of Metal Nanoparticles Inside Their Channels. J. Mater. Chem. 2008, 18, 5782–5786.
23. Castillejos, E.; Debouttiere, P.-J.; Roiban, L.; Solhy, A.; Martinez, V.; Kihn, Y.; Ersen, O.; Philippot, K.; Chaudret, B.; Serp, P. An Efficient Strategy To Drive Nanoparticles into Carbon Nanotubes and the Remarkable Effect of Confine- ment on Their Catalytic Performance. Angew. Chem., Int. Ed. 2009, 48, 2529–2533.
24. La Torre, A.; Rance, G. A.; El Harfi, J.; Li, J.; Irvine, D. J.; Brown, P. D.; Khlobystov, A. N. Transport and Encapsulation of Gold Nanoparticles in Carbon Nanotubes. Nanoscale 2010, 2, 1006–1010.
25. Castillejos, E.; Chico, R.; Bacsa, R.; Coco, S.; Espinet, P.; Perez- Cadenas, M.; Guerrero-Ruiz, A.; Rodriguez-Ramos, I.; Serp, P. Selective Deposition of Gold Nanoparticles on or Inside Carbon Nanotubes and Their Catalytic Activity for Preferential Oxidation of CO. Eur. J. Inorg. Chem. 2010, 5096–5102.
26. Rosenfeld, G.; Morgenstern, K.; Beckmann, I.; Wulfhekel, W.; Laegsgaard, E.; Besenbacher, F.; Comsa, G. Stability of Two- Dimensional Clusters on Crystal Surfaces: From Ostwald Ripening to Single-Cluster Decay. Surf. Sci. 1998, 402, 401–408.
27. Morgenstern, K.; Rosenfeld, G.; Laegsgaard, E.; Besenbacher, F.; Comsa, G. Measurement of Energies Controlling Ripening and Annealing on Metal Surfaces. Phys. Rev. Lett. 1998, 80, 556–559.
28. Meyer, R.; Ge, Q.; Lockemeyer, J.; Yeates, R.; Lemanski, M.; Reinalda, D.; Neurock, M. An Ab Initio Analysis of Adsorp- tion and Diffusion of Silver Atoms on Alumina Surfaces. Surf. Sci. 2007, 601, 134–145.
29. Heilmann, A.; Werner, J. In Situ Observation of Microstruc- tural Changes of Embedded Silver Particles. Thin Solid Films 1998, 317, 21–26.
30. Wynblatt, P.; Gjostein, N. A. Particle Growth in Model Supported Metal-Catalysts 0.1. Theory. Acta Metall. 1976, 24, 1165–1174.
31. Zhu, L.; Lu, G.; Mao, S.; Chen, J.; Dikin, D. A.; Chen, X.; Ruoff, R. S. Ripening of Silver Nanoparticles on Carbon Nano- tubes. NANO 2007, 2, 149–156.
32. Brust, M.; Walker, M.; Bethell, D.; Schiffrin, D. J.; Whyman, R. Synthesis of Thiol-Derivatized Gold Nanoparticles in a 2-Phase LiquidLiquid System. J. Chem. Soc., Chem. Commun. 1994, 801–802.
33. Rance, G. A.; Marsh, D. H.; Bourne, S. J.; Reade, T. J.; Khlobystov, A. N. van der Waals Interactions between Nanotubes and Nanoparticles for Controlled Assembly of Composite Nanostructures. ACS Nano 2010, 4, 4920– 4928.
34. Luo, Z.; Somers, L. A.; Dan, Y.; Ly, T.; Kybert, N. J.; Mele, E. J.; Johnson, A. T. C. Size-Selective Nanoparticle Growth on Few-Layer Graphene Films. Nano Lett. 2010, 10, 777–781.

Supporting Information

Assembly, Growth and Catalytic Activity of Gold Nanoparticles in Hollow Carbon Nanofibres

Alessandro La Torre,[a] Maria del Carmen Giménez-López,[a] Michael W. Fay,[b] Graham A. Rance,[a] William A. Solomonsz,[a] Thomas W. Chamberlain,[a] Paul D. Brown[c] and Andrei N. Khlobystov[a]

[a] *School of Chemistry, University of Nottingham, University Park, Nottingham, NG7 2RD, U.K.*

[b] *Nottingham Nanoscience and Nanotechnology Centre, University of Nottingham , University Park, Nottingham, NG7 2RD, U.K.*

[c] *Division of Materials, Mechanics and Structures, Department of Mechanical, Materials and Manufacturing Engineering, Faculty of Engineering, University of Nottingham, University Park, Nottingham, NG7 2RD, UK.*

S1. Synthesis and characterisation of 2.3 nm alkanethiolate-stabilised gold nanoparticles

The synthesis of dodecanethiolate-stabilised AuNPs was performed using a modified Brust–Schiffrin protocol.[33] To an aqueous solution of tetrachloroauric acid trihydrate (0.2 mmol) in deionised water (30 mL) was added a solution containing tetraoctylammonium bromide (0.4 mmol) in toluene (60 mL) and the mixture was vigorously stirred at room temperature for 10 min. To this mixture was added a solution containing dodecanethiol (0.2 mmol) in toluene (10 mL) and the mixture was vigorously stirred at room temperature for 10 min. To the reaction mixture was added a further solution containing sodium borohydride (2.0 mmol) in deionised water (30 mL) and the resulting mixture was vigorously stirred at room temperature for 20 hours. The biphasic mixture was then separated, retaining the organic layer that was washed with water (3 x 100 mL) and dried over anhydrous sodium sulphate. This was further purified by gentle centrifugation (5000 x *g*, 10 min), the supernatant removed, concentrated (*c.a.* 5 mL) under vacuum and the product precipitated from solution by addition of ethanol (350 mL) and storing at -30˚C for 24 hours. The resulting

precipitate was filtered through a 0.45 μm pore size PTFE membrane, the solid washed with ethanol (250 mL) and acetone (250 mL) and finally dried under vacuum to yield a brown solid product (38 mg AuNP).

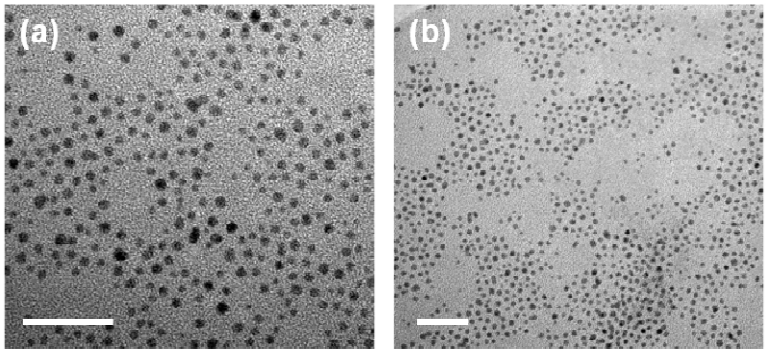

Figure S1. Bright field TEM images of dodecanethiolate-stabilised gold nanoparticles.

S2. Insertion of AuNPs into GNFs using supercritical CO_2

Graphitised carbon nanofibres (PR 24, 5 mg) were heated at 500 ˚C for 30 min in air, cooled down to room temperature and added to a suspension of dodecanethiolate-stabilised AuNPs (2.0 mg) in *n*-pentane (5 mL) under an inert atmosphere of argon. The resulting mixture was treated with ultrasound at room temperature for 30 min, transferred into a steel autoclave and mixed with carbon dioxide (40 ^{o}C, 4000 psi) for 18 hr. During the course of the experiment, the CO_2 pressure was cycled between 900 and 4000 psi three times. The resulting suspension was filtered through a PTFE membrane filter (pore size 0.45 μm), washed with *n*-pentane, ethanol and finally acetone to yield a black solid product (6 mg).

S3. Description of the vacuum system used for thermal evolution of AuNPs on GNFs

The vacuum system is designed to allow samples to be sealed in Pyrex glass tubes at low pressure (10^{-6} mbar). It is a two-stage system, which initially requires a roughing oil rotary pump to reduce the pressure to 10^{-3} mbar, followed by a turbo pump that reduces the pressure to 10^{-6} mbar. The sample is then sealed in the glass tube using a blowtorch under dynamic vacuum.

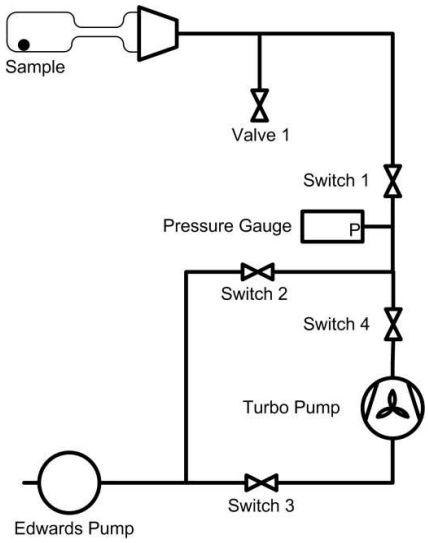

Figure S2. Schematic representation of the vacuum system used to seal AuNP-GNF samples in glass ampoules.

S4. Sealing of AuNP-GNF in glass tubes under vacuum

Pyrex glass tubes were thoroughly cleaned and dried. One end of the tube was sealed with a blowtorch and then the sample was added. Once the sample was at the sealed end of the tube, the middle of the tube was heated and drawn out into a narrow capillary. The tube was then allowed to cool. The metal screw cap, the flanged collar and the silicon o-ring were passed over the glass tube. The open end of the glass tube was inserted into the vacuum station and the metal cap was screwed until finger tight. The tube was evacuated to 10^{-6} mbar and sealed off with a blowtorch.

S5. Heating of the samples on a TEM grid sealed under vacuum

The AuNP-GNF composite sample was deposited onto a TEM grid and the grid was then sealed under vacuum at $5 \cdot 10^{-6}$ mbar in a Pyrex tube, as described above, and heated in a tube furnace for 2 hours at 300 °C.

S6. Heating of the bulk AuNP-GNF material sealed under vacuum.

The AuNP-GNF composite was sealed in a Pyrex tube at $5 \cdot 10^{-6}$ mbar and heated in a tube furnace for 2 hours at 300 °C.

S7. Thermal desorption of AuNPs from GNFs surface

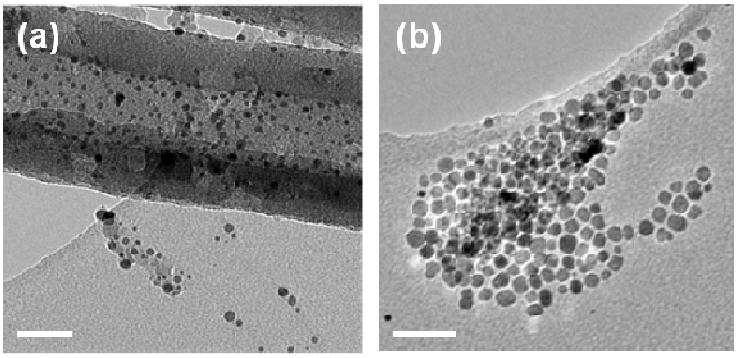

Figure S3. Bright field TEM images of AuNPs (13.5 ± 4.4 nm) that have been subjected to thermal desorption from the GNF outer surface during the heating of a AuNP-GNF sample on a TEM grid sealed under vacuum. Scale bars are 100 nm. TEM image acquisition was performed using an accelerating voltage of 100 kV.

S8. Ripening of AuNPs in GNFs activated by electron beam irradiation

AuNP-GNF composite was suspended in ethanol and sonicated for 10 minutes using a sonic probe (Sonics probe vibra@cell CV 18) at below 0 °C, and the formed mixture was filtered through a PTFE membrane. The composite was washed with THF, hexane, ethanol and acetone and dried under vacuum. The resulting black powder was deposited on a TEM support grid and heat-treated and analysed by *in situ* TEM.

The growth of nanoparticles was induced locally by condensing the 200 keV electron beam generated by a field emission electron gun source in a JEOL 2100F microscope down to a 300 nm diameter convergent spot, and observing the effect of the beam on the nanoparticles. The specimen was exposed to the condensed e-beam, supplying a current density of 50 pA/nm^2, for one minute after which the beam intensity was decreased to 7.2 pA/nm^2 for image acquisition. This process was repeated in order to build up a time-sequence of images that captures the various stages of the ripening process in action (Fig. S4).

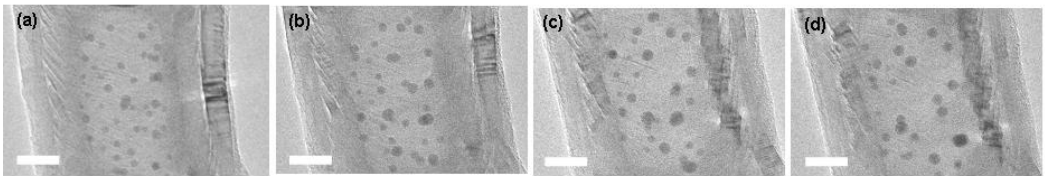

Figure S4. Bright field TEM images of a GNF filled with AuNPs, showing the growth of encapsulated AuNPs promoted by the 200 keV electron beam of the TEM after (a) 1 minute, (b) 10 minutes, (c) 30 minutes and (d) 120 minutes of exposure. Scale bars are 10 nm.

As can be seen, the total number of nanoparticles decreases whilst the mean size increases with time (Fig. S5). Nanoparticle growth activated by the convergent 200 kV electron beam (Fig. S4) is similar to that observed on the annular *in situ* TEM heated-stage at 100 kV.

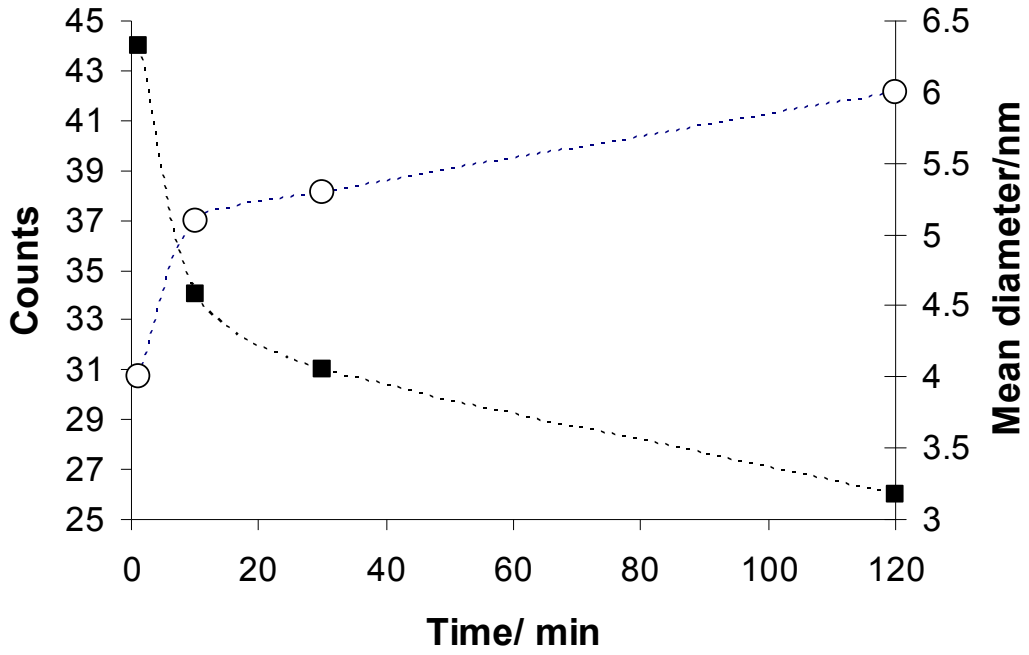

Figure S5. Change of the number of AuNPs and their mean diameters during the first two hours of the growth process triggered by irradiation with the 200 kV electron beam.

S9. *In situ* TEM measurements in real time

In an *in situ* TEM experiment the AuNP-GNF sample was prepared by casting several drops of a methanolic suspension of the composite onto either a copper or nickel grid mounted "holey" carbon films and drying under a stream of nitrogen. The annular-ring used for the *in situ* TEM experiment was a Gatan 652 double tilt-heating holder.

The sample was heated to 300 °C for 2 hour in the TEM column (Supplementary Video file). TEM image acquisition was performed using an accelerating voltage of 100 kV.

S10. X-ray photoelectron spectroscopy (XPS) measurements and thermal gravimetric analysis (TGA) for AuNP-GNF composites

Table S1. Quantification of the detected elements based on the XPS peak areas in the summed wide scans from three samples for pristine GNFs, AuNP-GNF before and after vacuum treatment at 300 ºC. All the elements are accounted for some contamination from the glass ampoule.

Samples	C1s %	O 1s %	S 2p %	B 1s%	F 1s %	N 1s %	Si 2p %	Au 4f %
GNFs	95.8	2.7	0	0.5	0	0.5	0.4	0
AuNP-GNF Before	83.4	4.2	1.5	0.5	0.9	0.5	4.0	5.0
AuNP-GNF After	85.7	7.9	0	0.3	0.9	0.5	4.3	0.4

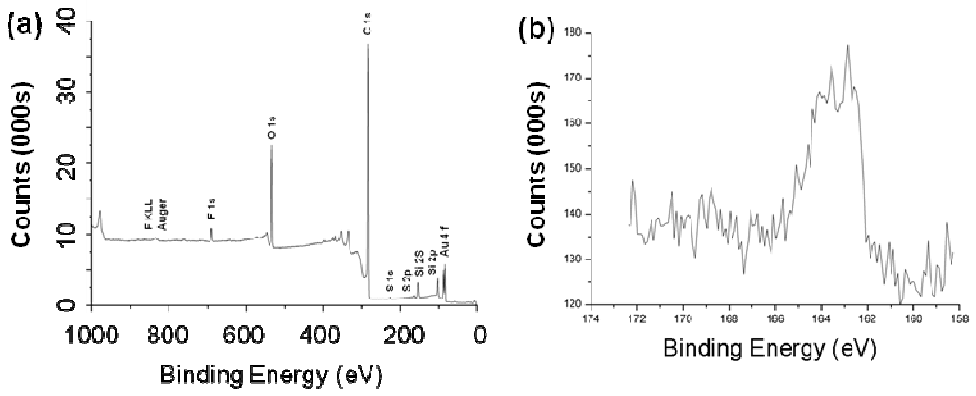

Figure S6. Wide scan XPS spectrum of AuNP-GNF before treatment in vacuum at 300 ºC (a) and high resolution XPS spectrum for the S *2p* signal of AuNP-GNF before treatment in vacuum at 300 ºC (b). The high resolution peak has been charge corrected to C *1s* at 284.7 eV (based on the carbon peak position of the GNF).

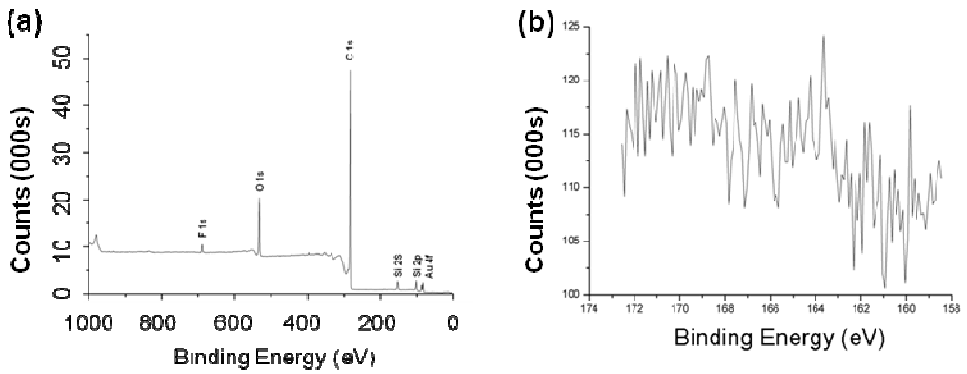

Figure S7. Wide scan XPS spectrum of AuNP-GNF after treatment in vacuum at 300 ºC (a) and high resolution XPS spectrum of the area of the S *2p* signal of AuNP-GNF after treatment in vacuum at 300 ºC (b). The high resolution peak has been charge corrected to C *1s* at 284.7 eV (based on the carbon peak position of the GNF).

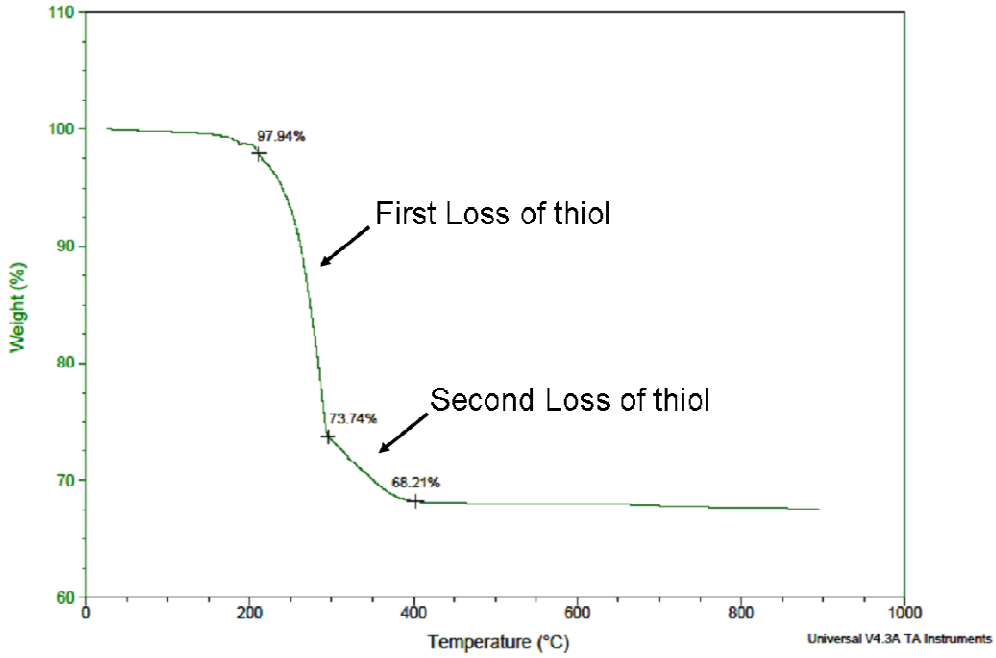

Figure S8. Thermal gravimetric analysis of 2.3 nm dodecanethiol stabilised AuNPs in air demonstrating that the majority of alkylthiol molecules are removed from the nanoparticles below 300 ^{o}C. In vacuum conditions, such as those used for the thermally activated growth of AuNPs, dodecanethiol is expected to vaporise and be removed from the sample at or below room temperature.

S11. Selective removal of the surface NPs and powder X-ray diffraction measurements for the resultant AuNP-GNF composite

AuNP-GNF composite (2 mg) thermal evolved in vacuum at 300°C and further heated at 300°C in air was added to ethanol (100 ml). The suspension was sonicated by a sonic probe (probe diameter 3 mm, frequency 20 KHz, power 130 W) for 15 minutes. The resultant suspension was filtered through a PTFE membrane filter (0.45 μm pore size), the solid product washed extensively with ethanol (250 mL) and acetone (250 mL), and dried in air to yield a black powder (1.6 mg).

Powder XRD pattern of the washed sample (Figure S11) shows a broad diffraction peaks for Au. Analysis of the peaks full width half maximum (FWHM) using the Sheerer equation indicates the average nanoparticle size 6.2 nm, which corresponds to AuNPs inside GNFs as observed by TEM imaging (Figure 6d). The bulk powder XRD confirms the efficient removal of larger AuNPs from GNF surface and retention of smaller AuNPs inside GNF.

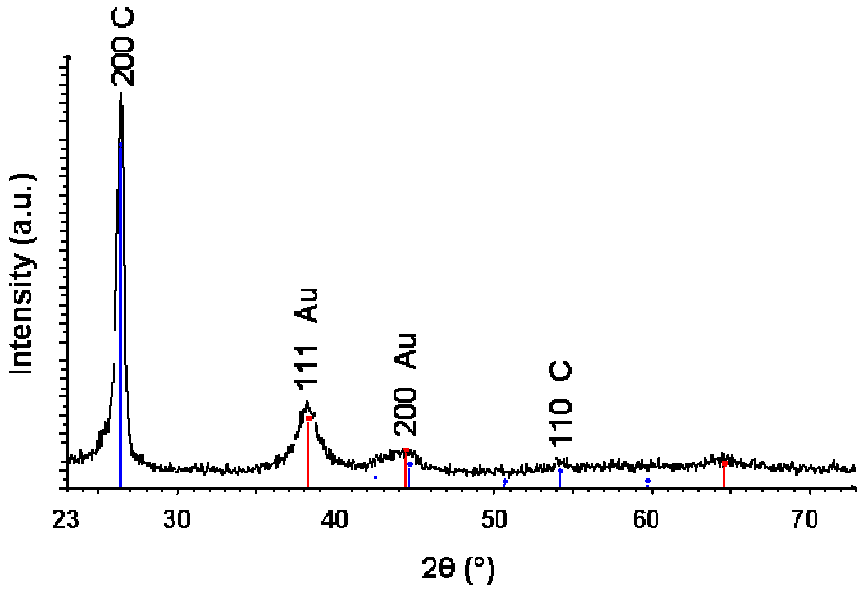

Figure S9. Powder XRD pattern for thermally evolved AuNP-GNF composite after the washing procedure.

S12. Oxidation of silanes catalysed by gold nanoparticles

The catalytic oxidation of dimethylphenylsilane[S1] by AuNP-GNF composites, where gold nanoparticles are either inserted into GNFs cavities ($AuNP_{int}$) or deposited onto their external surfaces ($AuNP_{ext}$) from solution, was carried out in a 10 mL glass vessel containing a magnetic stirrer bar. The procedure was as follows: the catalyst ($AuNP_{ext}$ or $AuNP_{int}$, 3.5 mg, 4.5 wt. % Au), dimethylphenylsilane (330 μmol, 50.6 μL) and acetonitrile (3 mL) were charged to the reaction vessel. The reaction was initiated by the addition of 30 % w/v aqueous solution of hydrogen peroxide (363 μmol, 46.0 μL) and the reaction mixture was left to stir at room temperature for 24 hours.[S2] The silanol and disiloxane products were then identified by GC-MS (VG Autospec in EI^+) mode of the crude mixture, and the relative quantities determined by comparisons of the peak areas.

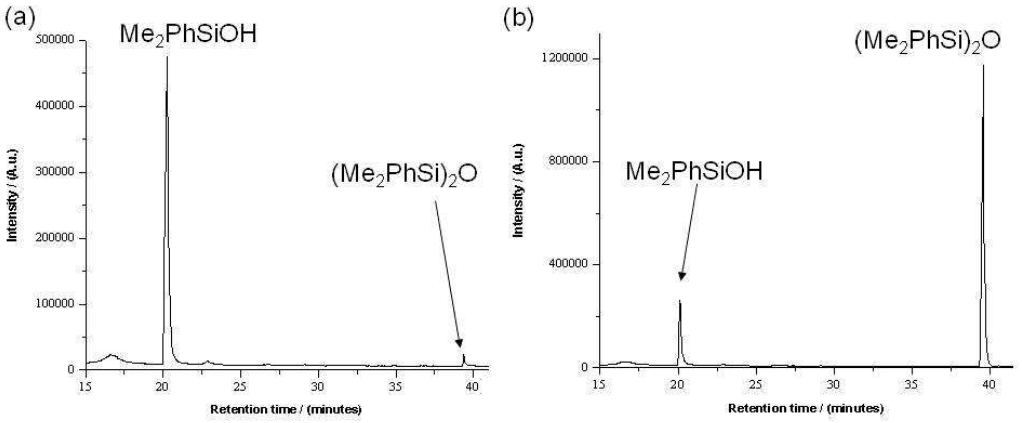

Figure S10. GC-MS chromatograms comparing the ratio of silanol **2** and siloxane **3** products for catalysist gold nanoparticles externally adsorbed on GNF $AuNP_{ext}$ (a) and encapsulated in GNF cavity $AuNP_{int}$ (b). Both reactions were carried out under the same conditions and for same duration of time as described above.

[S1] John, J.; Gravel, E.; Hagège, A.; Li, H.; Gacoin, T.; Doris, E. *Angew. Chem. Int. Ed.* **2011**, *50*, 7533.

[S2] Ishimoto, R.; Kamata, K.; Mizuno, N. *Angew. Chem. Int. Ed.* **2009**, *48*, 8900.